ELSEVIER

Contents lists available at ScienceDirect

Materials Today Communications

journal homepage: www.elsevier.com/locate/mtcomm





A soft syntactic foam actuator with high recovery stress, actuation strain, and energy output

Siavash Sarrafan, Xiaming Feng^{*}, Guoqiang Li^{*}

Department of Mechanical & Industrial Engineering, Louisiana State University, Baton Rouge, LA 70803, USA

ARTICLE INFO

Keywords:

- A. Foams
- A. Smart materials
- A. Thermosetting resin
- B. Thermomechanical

ABSTRACT

Novel syntactic foams were prepared by incorporating three types of glass microbubbles in a crosslinked cis poly (1,4-butadiene) (cPBD) matrix. The as-prepared semi-crystalline polymer-based syntactic foams displayed a clear two-way shape memory effect (2W-SME) with remarkable strain actuation of about 56% expansion when the temperature drops from 60 °C to -40 °C, and about 40% contraction when the temperature rises from -40 °C to 60 °C, comparable to most pure two-way shape memory polymers. Compared to the pure cPBD, which was actuated under 0.32 MPa tensile stress, the foams were actuated under a much larger external tensile stress of up to 1.6 MPa, signifying its superior actuation capability. The energy output is also much higher for the syntactic foam, up to 0.83 MJ/m³, compared to 0.28 MJ/m³ for the pure cPBD. Furthermore, it has a working temperature below zero Celsius and may be actuated at temperatures lower than most other available shape memory polymer foams. With a low density, decent mechanical properties, and great actuation capability, these syntactic foams can be adopted for applications such as artificial muscles, biomedical devices, soft robots, sealants, and aerospace structures, which can be potentially manufactured by 3D printing.

1. Introduction

Shape memory polymers (SMPs) are a class of polymers that can be programmed to keep a temporary shape and be triggered by mechanisms such as heat or light to switch to the original shape [1]. While one-way shape memory polymers can memorize only one temporary shape, two-way shape memory polymers can memorize two different shapes and can repeatedly shift between the two states. Since the introduction of two-way (2W) SMPs in 2001 [2], many polymers have been developed with the two-way shape memory effect (2W-SME). However, very few of them function in low temperatures. By 2018, there had been only one polymer that could be used in temperatures below 0 °C, and the lowest operating temperature was - 20 °C [3]. However, its actuation strain was limited to only 30% under tension. In 2018, our group reported a 2W-SMP based on crosslinked cis polybutadiene (cPBD) that exhibited an impressive 2W-SME under a maximum tensile load of 0.32 MPa [4]. The cPBD could actuate with an expansion upon cooling (EUC) and contraction upon heating (CUT) over 100%, when temperature cycles between - 40 and 60 °C. More remarkably, this 2W-SMP could function at temperatures much lower than most other 2W-SMPs developed to date. Although the already developed 2W-SMPs exhibit excellent actuation strain, achieving a higher actuation stress could be a substantial improvement as it makes the material even more attractive for applications such as sealants [5,6], artificial muscles [7,8], and self-healing [9].

Since the advent of polymeric foams in 1931 [10], many foams have been developed by introducing empty pockets or a gas inside liquid or solid polymer matrices. Adding gas, such as air [11], nitrogen [12], or carbon dioxide [13,14], or incorporating hollow spaces may significantly reduce the density of the final material while enhancing its shock absorption and thermal insulation properties. Due to the interesting properties of SMPs, many researchers exploited them to develop SMP foams. For example, polystyrene [15], polyurethane [16,17], epoxy [18], polycaprolactone [19] and polybutadiene [20] have all been used in SMP foams. Another method to create a polymer foam is by mechanically dispersing bubbles or particles made of metals, ceramics, or polymers into a polymer matrix. This type of foam is called syntactic foam. Compared with pure polymer foams, either open-celled or close-celled, syntactic foams are usually stronger, making them attractive in structural applications. Like other composites, the mechanical and physical properties of this special type of particulate-filled polymer composites (PFPC) can be tailored for a particular purpose. The

E-mail addresses: xfeng@lsu.edu (X. Feng), lguoqi1@lsu.edu (G. Li).

^{*} Corresponding authors.

SMP-based syntactic foams are highly engineerable for a specific application and show greater specific strength compared to normal SMPs. As a result, these materials are widely used in industries such as aerospace and underwater vehicles that weight or tunability is of high importance. To combine the unique features of both SMPs and PFPCs, many SMP-based syntactic foams are developed to date [21–24]. These materials are extensively studied as sandwich cores [25,26] or in acoustic applications [27].

Although pure cPBD has exhibited excellent 2W-SME even at frozen temperatures, the main limitation persists in its small actuation stress. If its actuation stress can be further increased and its density can be reduced, it will find many applications in lightweight structures and devices, particularly in cold environments. In this study, a novel syntactic foam with hollow glass microspheres (HGMs) dispersed in cPBD matrix was prepared and tested. HGMs are chemically inert, inexpensive, and have a low coefficient of thermal expansion. These unique properties have made them one of the most widely used hollow fillers available. Three types of HGMs were utilized with a fixed volume fraction of 40%. The physical, chemical, mechanical, and 2W-SME were characterized, and governing mechanism was discussed.

2. Experiments

2.1. Raw materials

Cis poly(1,4-butadiene) (PBD) under the trade name Budene 1208 was purchased from Goodyear, USA. Its viscosity is 46 (Mooney mL 1 + 4@100 °C). Its onset glass transition temperature is - 104 °C. Dicumyl peroxide (DCP) was purchased from Acros Organics (Geel, Belgium). Three types of soda-lime-borosilicate glass composition HGMs, K1, K15, and K20, purchased from 3 M (Saint Paul, MN) with true densities of 0.125 g/cm³, 0.15 g/cm³, and 0.20 g/cm³, respectively, were used as the microfillers. The isostatic crush strength of the three bubbles is reported as 1.72 MPa, 2.07 MPa, and 3.45 MPa, in the same order as their densities. Their median particle diameter is 65 μ m, 60 μ m, and 60 μ m, respectively. Chloroform was purchased from VWR (Radnor, PA).

2.2. Preparation of syntactic foams

First, 5% PBD solution was prepared by immersing small pieces of PBD in chloroform at a 5-95 wt ratio. It was gently mixed once per day for seven days and then blended briskly using an overhead stirrer to form homogenous consistency. After that, 40% by volume of GHMs was added to the solution, together with DCP of 3% by weight of PBD. The completely uniform mixture was then poured into circular aluminum molds and left for 24 h under a ventilated fume hood for the chloroform to be evaporated. It was then removed from the mold and placed in a vacuum chamber for another 24 h to thoroughly remove the chloroform. The resulted thin film was then folded and pressed for 24 h to obtain samples of the desired thickness. This step also eliminated small pockets created by evaporation of the chloroform solvent. The final samples were then cured in an oven at 150 °C for 30 min. In the following, the pure cPBD samples are named PBD for short. The syntactic foams are named K1PBD, K15PBD, and K20PBD, respectively, depending on the type of HGM used.

2.3. Characterizations

The density of the three foams was determined by measuring their volume and weight. The volume of the syntactic foam was measured by the water displacement method. Weight of the specimens was measured using an XS105 scale by Mettler (Toledo, Italy). The density was then calculated based on the measured weight and volume. Reported results are calculated based on average measurements of three pieces of samples from each type of foam.

The thermal properties of the foams were characterized by DSC.

Samples of approximately 5 mg were placed in aluminum pans and placed in a DSC 4000 calorimeter by PerkinElmer (Waltham, MA) and scanned from - 60 to 60 $^{\circ}$ C. The heating and cooling rates were set to be 10 $^{\circ}$ C/min, and the nitrogen gas flow was chosen as 20 mL/min. To eliminate the thermal history of the specimens, the second heating and cooling cycles were plotted.

Dynamic mechanical analysis (DMA) was performed using a Q800 DMA by TA Instruments (New Castle, DE) to determine the thermomechanical properties of the developed syntactic foams. A temperature sweep was done in multi-frequency/strain mode from $-40\ \text{to}\ 80\ ^\circ\text{C}$ with a linear rate of 3 $^\circ\text{C/min}$. The frequency was set to be 1 Hz, and the amplitude was chosen to be 20 μm . Rectangular-shaped films of the three types of foams with an effective length of 5.5 mm, a width of 1.5 mm, and a thickness of 2 mm were used under tension mode.

DMA was also utilized to study the 2W-SME by applying a constant external force to the foams and recording the resulted elongation during multiple thermal cycles through controlled force mode. 5.5 mm \times 1.5 mm \times 2 mm films of the three types of foams were used under tension. Under each tensile load, the temperature was cycled several times from - 45 to 60 °C with a heating and cooling rate of 5 °C/min.

Tensile tests were conducted using an eXpert 2610 Universal Testing Machine (UTM) by ADMET (Norwood, MA). Two separate tensile tests were performed. One at room temperature and the other at $-40\,^{\circ}\text{C}$. An F-280DT ADMET environmental chamber, controlled by an Omron E5AC-T digital controller (Kyoto, Japan), was used for the low-temperature test (Fig. S1). For both tests, the displacement speed was $10\,\text{mm/min}$. Specimens were made by cutting sheets of 2 mm thick foam using a cutter shaped as the standard-sized dog bone (ASTM D638 IV) (Fig. S2). Reported results are based on the average of three tests, with each selected from a different batch of cured polymer.

Scanning electron microscopy (SEM) was used to observe the distribution of glass bubbles in the syntactic foams. Small specimens were first covered with a 50 nm layer of gold using a Vacuum Sputter by Denton (Moorestown, NJ) to establish better conductivity with the carbon surface of the stub. A Phenom ProX Desktop SEM (Eindhoven, The Netherlands) was used to capture the images. The accelerating voltage was 15 kV, and the working distance was 9–9.5 mm.

Fourier-transform infrared spectroscopy (FTIR) was used to characterize the chemical structure of syntactic foams. A Nicolet iS10 spectrometer manufactured by Nicolet Instrument Corporation (Madison, WI) was used to test samples in a range of 4000–400 $\rm cm^{-1}$.

Thermogravimetric analysis (TGA) of the developed foams was conducted using a TGA 550 machine made by TA Instruments (New Castle, DE). The typical thermogram was recorded from room temperature to 800 $^{\circ}\text{C}$ at a rate of 10 $^{\circ}\text{C}/\text{min}$ under a nitrogen atmosphere.

The rheological studies were performed using a Discovery HR 30 rotational rheometer manufactured by TA Instruments (New Castle, DE). The geometries of the test fixtures were parallel disks with a diameter of 25 mm. Frequency sweep test was conducted at room temperature. The temperature sweep of the foams was performed at a heating rate of 3 $^{\circ}\text{C/min}$ from - 10 to 60 $^{\circ}\text{C}$.

3. Results and discussions

3.1. Characterization of structure and morphology

The measured density is given in Table 1. In Table 1, the theoretical density is based on the general rule of mixtures approach, i.e., the

Table 1The measured density of the pure polymer and foams.

	PBD	K1PBD	K15PBD	K20PBD
Theoretical Density (g/cm ³⁾ Actual Density (g/cm ³⁾ Additional porosity (%)	0.9	0.689	0.696	0.711
	0.823	0.637	0.643	0.660
	8.5	7.5	7.6	7.2

weighted mean of the component. From Table 1, the theoretical and measured densities for the four materials are close. The slight difference between the theoretical and measured densities can be attributed to the entrapped air in the prepared samples. The additional porosity was calauclated as {Additional porosity (%) = [(theoretical density – experimental density)/theoretical density] \times 100%}. The additional porosity due to entrapped air bubbles was calculated and is given in Table 1. Based on Table 1, the additional porosity of the prepared foam specimens is slightly lower than that of the PBD and the quality is acceptable.

Fig. 1 is a typical SEM image of the foams after specimen preparation. It depicts that the glass bubbles are evenly distributed and take approximately 40% of the volume of the PBD matrix. As the comparison between the measured and theoretical densities suggested, the majority of the entrapped air and gas were removed during the preparation process. This was further validated by the absence of large air pockets in the SEM images. The SEM image also shows that a limited number of glass bubbles were damaged during preparation, possibly by mixing or pressing. The number of broken bubbles appears to be greater on the outer surface of specimens, which was in contact with the external compressive load.

To further examine the preparation process, the load applied by the presser was simulated on smaller pieces of syntactic foam using the MTS machine. It was determined that the K1PBD, K15PBD, and K20PBD samples took a compressive stress of approximately 2.5 MPa, 3 MPa, and 3.2 MPa, respectively. It is also believed that due to the viscoelastic and viscoplastic properties of the PBD matrix with bubbles during the many hours of holding time, the presser load is probably distributed unevenly and the stress on glass bubbles is higher than the surrounding matrix. The large compressive force employed by the presser as well as

the mixing process may both be responsible for the rupture of some of the microbubbles. Therefore, alternative methods for mechanically dispersing the bubbles and improvements in forming the material may potentially result in even more superior foam properties.

Fig. 2 shows the FTIR results of as-prepared PBD, K1PBD, K15PBD, and K20PBD, respectively. Examining the identified characteristic peaks

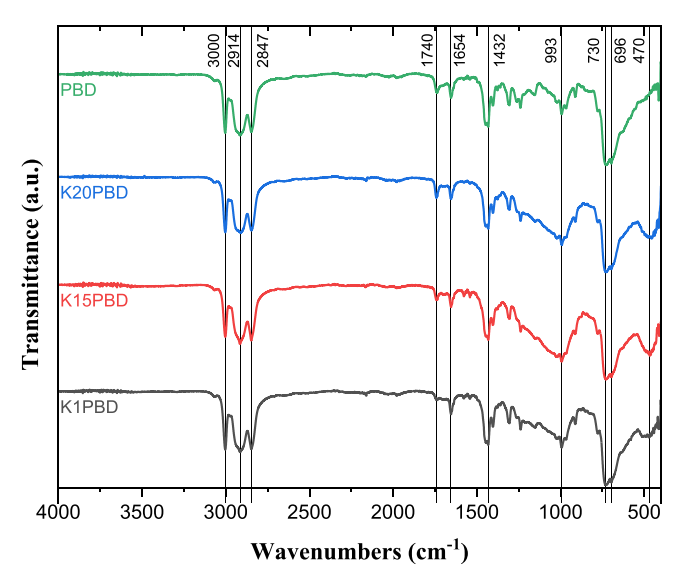


Fig. 2. FTIR spectrum of the developed syntactic foams compared to pure crosslinked PBD.

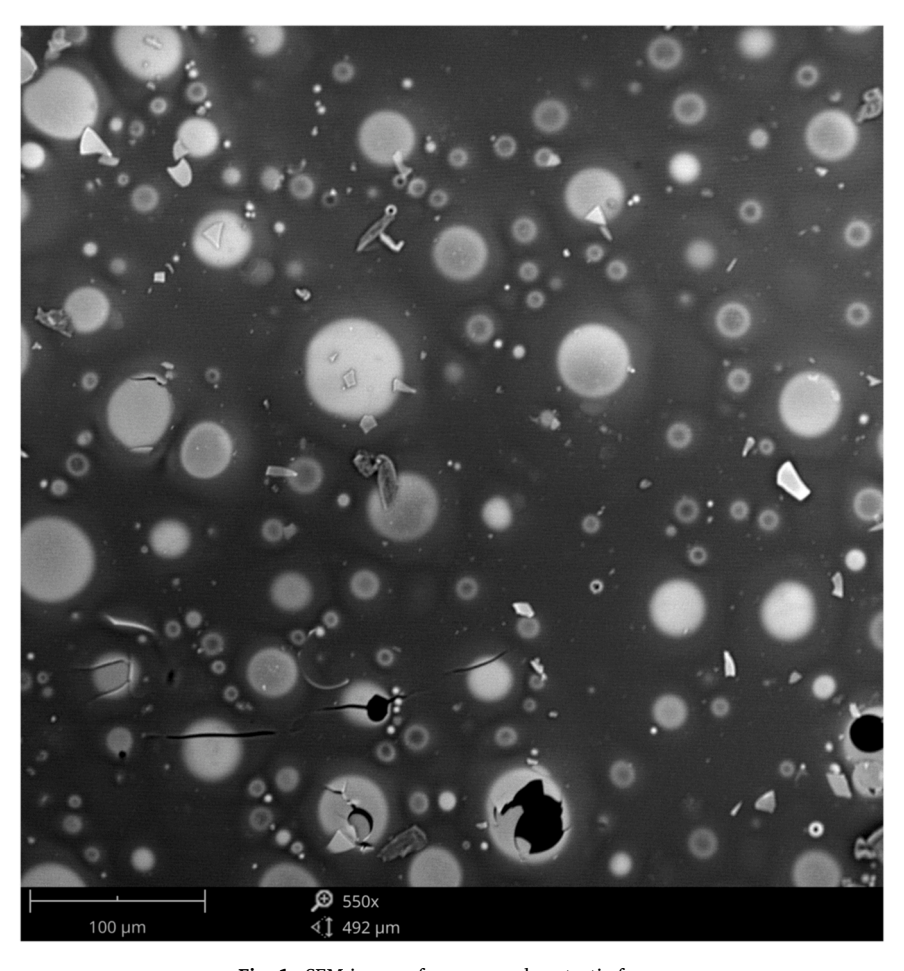


Fig. 1. SEM image of as-prepared syntactic foam.

marked in Fig. 2 indicates that the three syntactic foams exhibit a nearly identical FTIR profile to the crosslinked PBD. The sole exception is the peak detected at around 470 cm⁻¹, only observed in the specimens with glass microbubbles. This wavelength can be assigned to Si-O-Si bending, which is clearly due to the presence of glass bubbles. Otherwise, peaks and even intensities of the four specimen types were very similar. It suggests that the addition of glass bubbles does not alter the existing chemical bonds in the polymer. Therefore, the interfacial bonding between the microbubbles and the PBD matrix is purely physical. The comparison between the three syntactic foams further proves that the size and density of the microbubbles have essentially no impact on bond lengths and types.

3.2. Thermal behavior

The heat flow profiles during the second heating and cooling cycle are shown in Fig. 3 for the three syntactic foams. The melting temperature (T_m) and crystallization temperature (T_c), determined from the peak of the heat flow curve, were around -12 °C and -40 °C, respectively. Comparing these values with the numbers reported for pure crosslinked PBD, -8.7 °C and -34.9 °C (Fig. S3) [4], indicates that incorporating the hollow microbubbles into the PBD slightly decreases the crystallization and melting temperatures. The small difference between the reported T_m and T_c for the pure crosslinked PBD and the syntactic foams may be attributed to the potential dissimilarities in the synthesis and curing processes. For pure PBD, the enthalpy change in the endothermic peak is 30.3 J/g and the enthalpy change in the exothermic peak is -42.7 J/g [4]. The enthalpy changes (ΔH) of the endothermic peaks were calculated as 25.9 J/g, 22.1 J/g, and 18.7 J/g for K1PBD, K15PBD, and K20PBD, respectively. The enthalpy changes for exothermic peaks for the three syntactic foams were determined in the same order as -38.3 J/g, -29.3 J/g, and -24.9 J/g. From these results, it is seen that the degree of crystallization decreases in the order of K1PBD, K15PBD, and K20PBD, all of which are lower than that of the pure PBD. It demonstrates that the inclusion of glass bubbles could suppress the crystallization of PBD matrix due to the strong interfacial action between glass bubbles and PBD molecules, so called confined interfacial layer or interphase. Moreover, both the melting and crystallization temperatures are lower than the freezing temperature, suggesting that the foams may have 2W-SME at frozen temperatures.

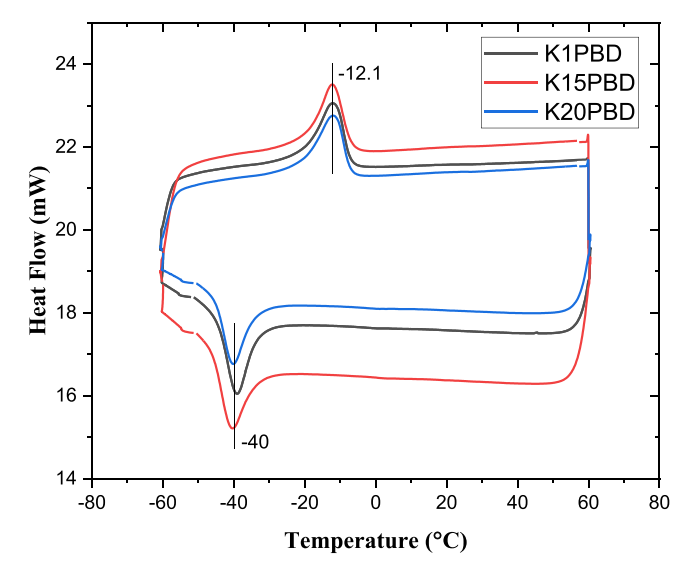


Fig. 3. DSC plots for the three syntactic foams.

3.3. Dynamic mechanical property

Storage modulus, loss modulus, and loss factor (tan δ) are plotted for the three syntactic foams in Fig. 4(a)–(c), respectively. The temperature corresponding to the peak of the tan δ is usually regarded as the transition temperature. In this slightly crosslinked thermoset, the transition is attributed to the melting temperature (T_m) and was observed at 11.62 °C, 7.90 °C, and 6.26 °C for K1PBD, K15PBD, and K20PBD, respectively. While the inconsistency between the T_m determined using DMA and DSC is justified by the clear differences in the measurement methods, the difference among the measured melting temperatures for the three foams using DMA results hints at the effect of microbubbles on the storage and loss moduli of the polymer. The T_m of the pure crosslinked PBD determined from DMA was reported to be around 16 °C [4]. With the incorporation of GHMs, an overall increase in the storage modulus of the foams was observed. At $-40\,^{\circ}$ C, the storage modulus can be identified as 200 MPa, 270 MPa, and 300 MPa for K1PBD, K15PBD, and K20PBD, respectively, as compared to the storage modulus of the PBD, which is 165 MPa [4]. Both storage and loss moduli reduce with heating and plateau after the melting temperature. The storage modulus at the plateau region is from 1 MPa to 6 MPa for the three syntactic foams. The one to two orders reduction in storage modulus signifies that the foams may have good shape memory effect, which has been well established for entropy-driven shape memory polymers [28]. Similar to the melting point, the storage modulus of the as-prepared syntactic foams was in the same order of magnitude as the pure crosslinked PBD, suggesting that the chemical composition and the shape memory mechanism are not significantly altered by adding the glass bubbles.

3.4. Two-way shape memory effect

Fig. 5(a) shows the maximum constant tensile load that can be applied to the pure crosslinked PBD during actuation, which was 0.32 MPa. However, the as-prepared syntactic foams based on PBD enhanced the applied load of the foam by several times. As shown in Fig. 5(b)-(d), incorporating K1, K15, and K20 glass microbubbles enabled the foams to carry loads of up to 0.75 MPa, 1.2 MPa, and 1.6 MPa, respectively. Therefore, the foams have much higher recovery stress than the PBD, suggesting that the foams can lift a much heavier load than the pure PBD when the temperature rises. Of course, the actuation strain of the foams was reduced. However, the output energy density by the foams, which can be approximately estimated as the product of the stress and strain based on a typical heating branch (the specimen lifts a constant weight by a certain distance), is about 0.28 MJ/m³, 0.41 MJ/m³, 0.55 MJ/m³, and 0.83 MJ/m³ for the PBD, K1PBD, K15PBD, and K20PBD, respectively. Therefore, the as-prepared foams not only have higher recovery or actuation stresses, but their ability to do work is also higher. Considering the foams are lighter than the PBD, the specific energy output (the energy output divided by density) and ability to lift weight are even higher for the foams than for the PBD. Movie S1 demonstrates the ability of a small stripe of foam to lift some weight repeatedly during several thermal cycles.

Supplementary material related to this article can be found online at doi:10.1016/j.mtcomm.2022.103303.

Fig. 5 also shows that the 2W-SME of the foams is triggered at both frozen temperatures and temperatures higher than the melting temperature, suggesting that both melting/crystallization transition and rubber elasticity endows the foams with 2W-SME [29]. The clear change in the slope of the actuation strain with respect to temperature in the cooling branch of each foam further validates that different mechanisms control this effect. Such behavior has been noticed for various 2W-SMPs, including ionomer [30], poly(ethylene-vinyl acetate) [31], polycaprolactone [24], and PBD [4].

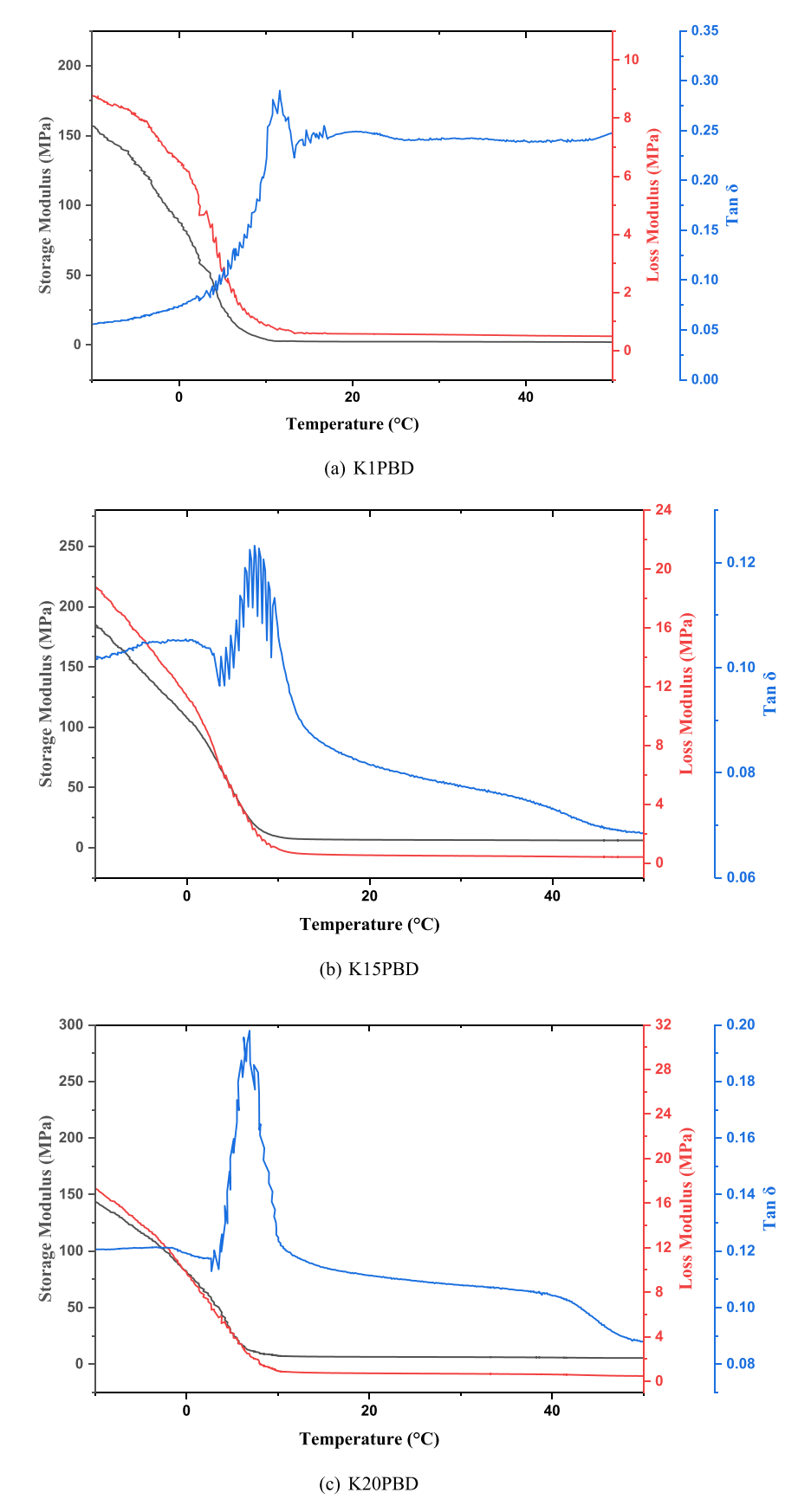


Fig. 4. Temperature sweep for (a) K1PBD, (b) K15PBD, and (c) K20PBD syntactic foams to show the change in storage modulus, loss modulus, and tan δ from - 20 to 80 °C.

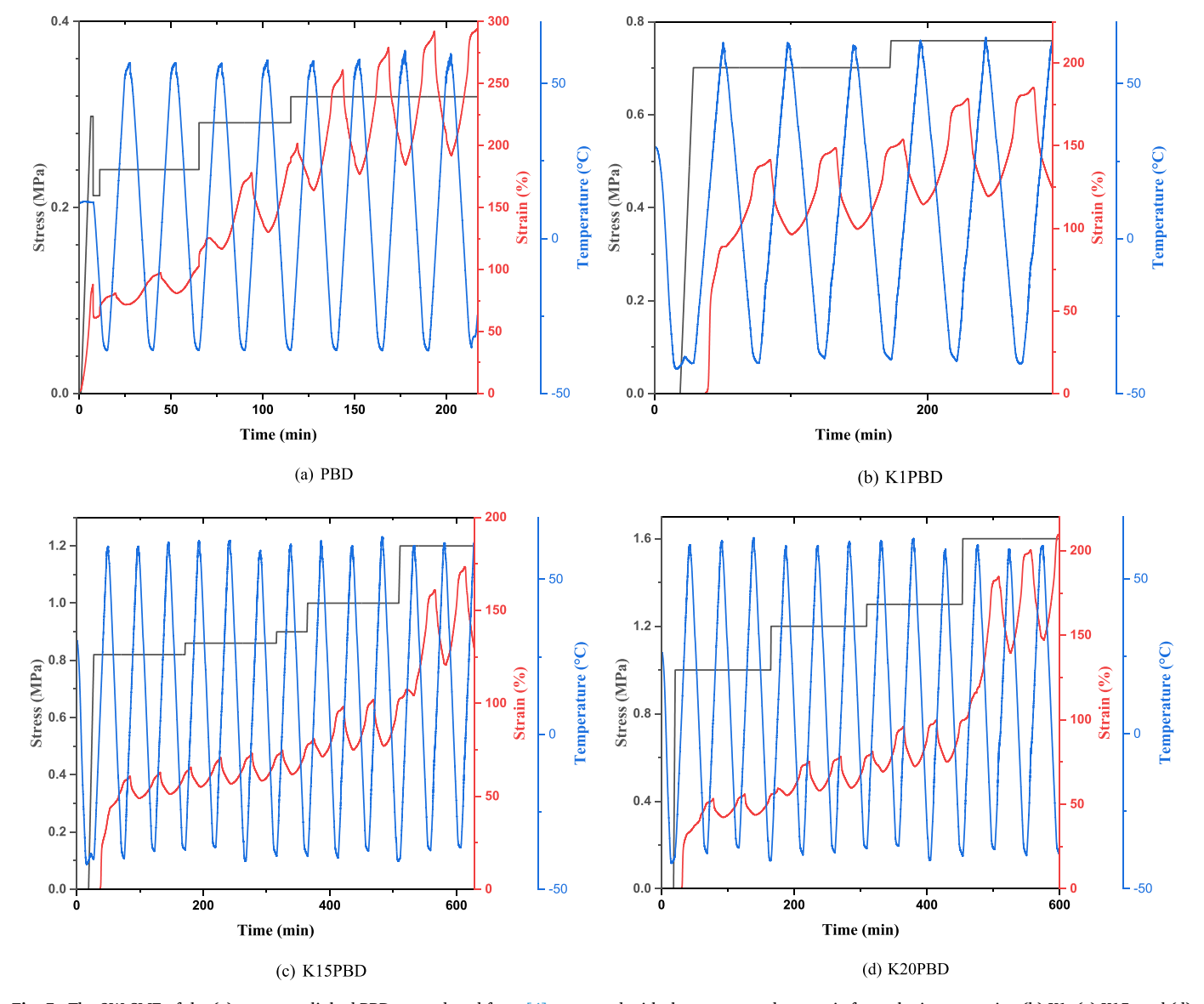


Fig. 5. The 2W-SME of the (a) pure crosslinked PBD, reproduced from [4] compared with the as-prepared syntactic foams by incorporating (b) K1, (c) K15, and (d) K20 glass microbubbles.

3.5. Mechanical properties

The tensile stress-tensile strain curves at room temperature are plotted for K1PBD, K15PBD, K20PBD, and pure PBD in Fig. 6. It is noticeable that incorporating the micro-glass bubbles into the cross-linked PBD matrix remarkably increased the strength and strain at rupture. The strength of the syntactic foam was found to be directly correlated to the strength of the glass bubbles. The maximum stress of the pure PBD at room temperature was merely 0.73 MPa at a fracture strain of roughly 207%. In comparison, the developed syntactic foams demonstrate strengths of 1.18 MPa, 2.23 MPa, and 2.71 MPa, with elongations at break equal to 569%, 803%, and 938%, respectively, for K1PBD, K15PBD, and K20PBD. In other words, the syntactic foams show an increase of up to 4.6 times in specific strength and approximately 4.5 times in the fracture strain at room temperature compared to the pure PBD.

All three syntactic foams demonstrated a non-linear behavior at smaller elongations and then entered into a pseudo-plastic region. A noticeable difference in the stress-strain curve of the syntactic foams from the pure PBD is that the strain softening in PBD does not lead to a second hardening region. Therefore, the ductility of PBD is limited.

However, the syntactic foams are particulate composites reinforced by particles with higher stiffness. This trend is typically observed for the stress-strain curves of rubbers compared to the reinforced rubbers [32]. The PBD is also in a rubbery state at room temperature. Due to the presence of spherical particles, stress concentration may develop in the vicinity of the inclusions. The stress and strain concentration, notably in the radial direction of the particles, could potentially increase the axial elongation at failure. This can be further explained as follows. The PBD based syntactic foams, like other syntactic foams, may have a very thin layer or interphase between the pure PBD matrix and the glass microsphere. During the curing process, the mobility of the PBD molecules within the interphase is restricted due to the surface tension of the glass microballoons. As a result, the interphase may have lower crosslink density than the pure PBD matrix. This type of interphase layer was identified in one of our previous studies on one-way shape memory polymer based syntactic foam by Xu and Li [33]. As is well-known, uncured PBD has huge ductility. Therefore, this interphase layer may significantly contribute to the much enhanced stretchability of the syntactic foams as compared to the pure crosslinked PBD at room temperature. This result can also be explained by another study. Li et al. [34] studied a three-layer built-in model. In this model, the unit cell was

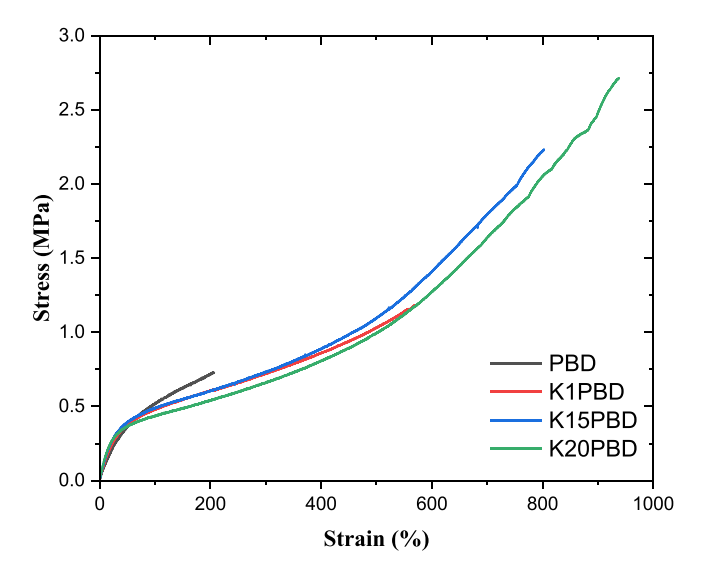


Fig. 6. Comparison between the stress-strain curves of K1PBD, K15PBD, K20PBD, and pure crosslinked PBD under uniaxial tension at room temperature.

a three-layer sphere, which was made of a stiff spherical core that was coted by a soft layer, and then further coated by a layer with stiffness in-between the stiff core and the soft interphase layer, similar to the syntactic foam studied here. Based on the modeling results, radial or axial strain concentration occurs in the soft layer, suggesting that the soft layer deforms significantly under axial tension. The glass microbubbles may also alter the heat distribution in the polymer during the curing process. Glass bubbles have a small thermal conductivity $(0.047~\text{W/m}~\text{K},\,0.055~\text{W/m}~\text{K},\,\text{and}\,0.070~\text{W/m}~\text{K}$ for K1, K15, and K20 glass bubbles, respectively), which may leave the polymer surrounding them to be not cured completely. The high deformability of the under-cured polymer, along with the induced strain concentration affecting the under-cured interphase, may both contribute to a higher elongation at break. The difference in the mechanisms during the fracture was also evident in the fracture surfaces of the foams. Visual inspection of the fracture surface shows that the crosslinked PBD had a smooth surface in the 90-degree plane, while the syntactic foams had dull and fibrous surfaces after breakage (Figs. S4 and S5). The modulus of the syntactic foams in the small strain region increases with the strength and density of the inclusion bubbles. This observation is consistent with previous findings for other polymeric syntactic foams [35].

The tensile stress-strain curves for K1PBD, K15PBD, and K20PBD syntactic foams and the pure cPBD at -40 °C are plotted in Fig. 7. The ultimate strengths were 27.68 MPa, 8.73 MPa, 9.19 MPa, and 13.76 MPa, while elongations at break were 529%, 263%, 194%, and 284%, for PBD, K1PBD, K15PBD, and K20PBD, respectively. Similar to the tensile tests performed at room temperature, stronger inclusions result in a stronger syntactic foam. However, the fracture strains of the three syntactic foams do not appear to be dependent on the type of glass bubble used. The latter suggests that the failure of the composite syntactic foams at temperatures below the crystallization point is probably due to the failure in the PBD matrix. Since $-40\,^{\circ}\text{C}$ is below the determined $T_{\rm c}$ of the crosslinked PBD, the matrix is stiffened, which may also be noticed by comparing the higher elastic modulus in these tests with the tests at room temperature. The composite may here be considered as a hard matrix with softer inclusions. Stress concentration in the vicinity of the microbubbles is now in the tangential direction of the particles and may initiate fracture in the matrix. However, the stronger pure crosslinked PBD is at the semi-crystalline state and can itself be regarded as a reinforced composite. Therefore, the ultimate tensile strength of the pure crosslinked PBD is higher than all three syntactic foams at this temperature. A small yielding region can also be noticed in all the stress-

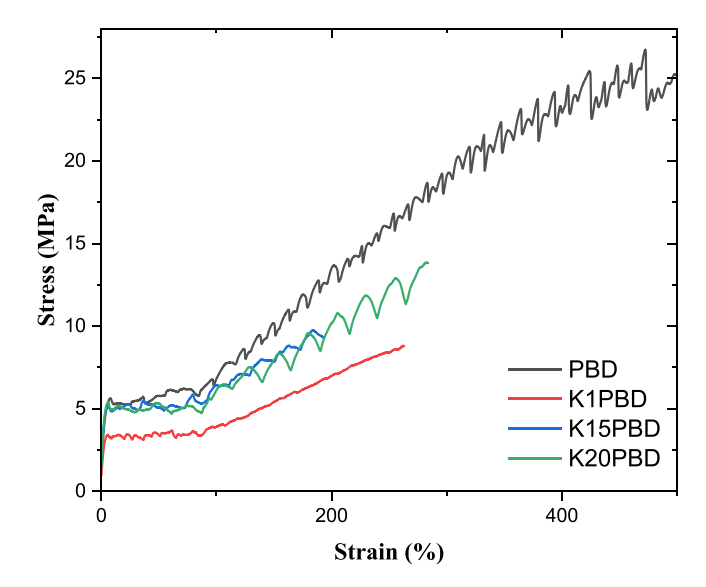


Fig. 7. Comparison between the stress-strain curves of K1PBD, K15PBD, K20PBD, and pure crosslinked PBD under uniaxial tension at - 40 $^{\circ}$ C.

strain curves at $-40\,^{\circ}$ C. This yielding is due to the coordinated segmental rotation taking place in the PBD matrix that is in the glassy state at this temperature.

3.6. Thermal stability

Fig. 8 shows the thermal degradation initiates around 200 $^{\circ}$ C in all samples and peaks at 450 $^{\circ}$ C from the TGA test. Since PBD autoignition temperature is around 450 $^{\circ}$ C [36,37], the peak degradation of the samples can be attributed to the degradation of the PBD matrix. It was also observed that the glass bubbles with higher density (e.g., K20) lead to higher residue at 800 $^{\circ}$ C. This correlation suggests that the glass bubbles were probably the only components left in the samples at temperatures above the decomposition temperature of PBD. K1PBD, K15PBD, and K20PBD each experience a weight loss of 95%, 88%, and 83% at this stage, respectively.

3.7. Viscoelasicity

The complex viscosity with angular frequency and with temperature are shown in Fig. 9(a) and (b), respectively. Besides the increased complex viscosity due to the addition of glass bubble fillers, it is seen that, with the increase in angular frequency, the viscosity of the cross-linked PBD and foams decrease. This shows that both the crosslinked PBD and foams have shear thinning properties. Shear-thinning is a desired properties for certain applications, such as in extrusion based 3D printing. As expected, the complex viscosity decreases as temperature rises. The incorporation of HGMs increases the complex viscosity, which again is expected.

4. Conclusions

Three types of novel two-way shape memory syntactic foams made of crosslinked cis polybutadiene and hollow glass microbubbles were reported. It was shown that the incorporation of glass bubbles remarkably increased the load to trigger 2W-SME while decreasing the density and enhancing several other mechanical and physical properties of the crosslinked PBD. Notably, adding the K20 glass bubbles was shown to obtain the most superior 2W-SME with actuation under a maximum tensile load of 1.6 MPa, and maximum energy output of 0.83 MJ/m³ in the heating branch. Due to the unique actuation range of -45 to $60\,^{\circ}$ C, significant load to weight ratio, enormous reversible EUC/CUH, and

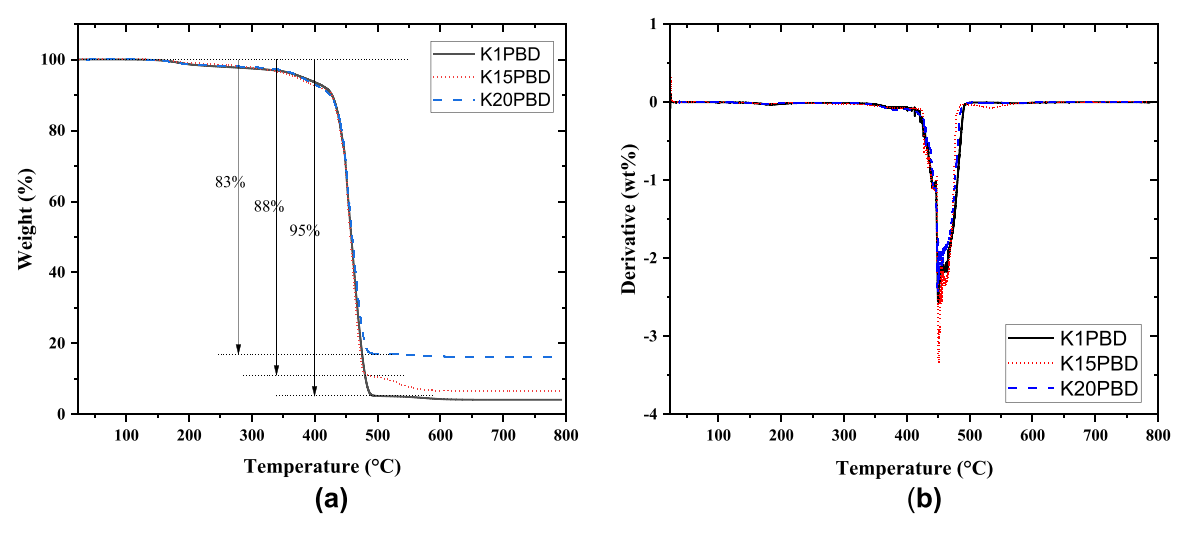


Fig. 8. (a)Thermogram plot (TG) and (b) Derivative of the thermogravimetric (DTG) curves for the three developed syntactic foams.

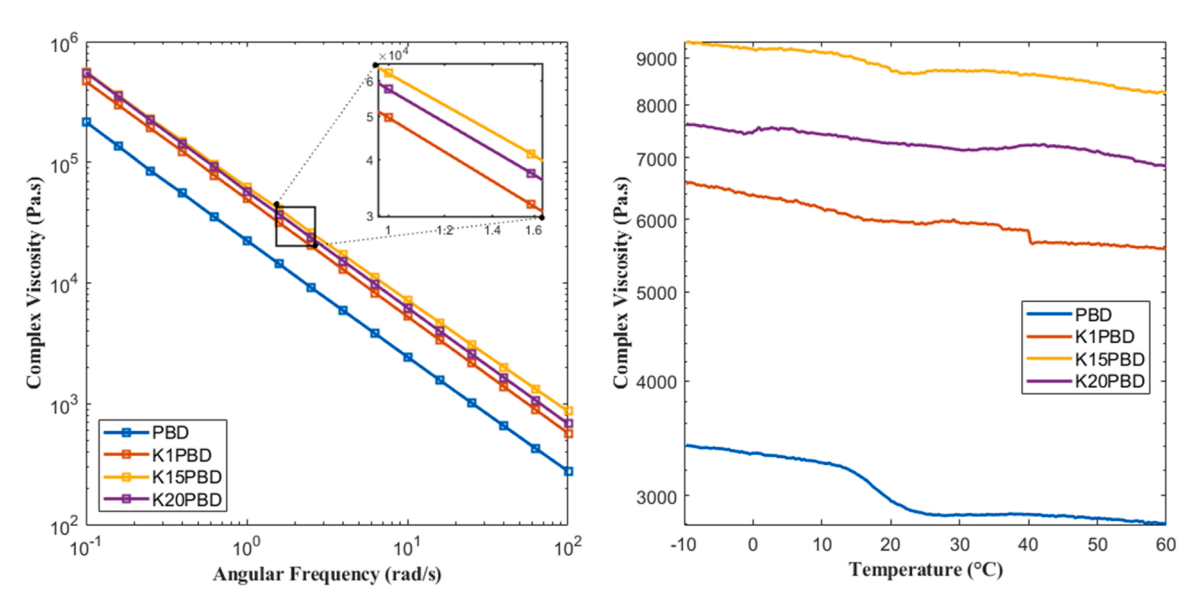


Fig. 9. Complex viscosity for the three syntactic foams and the crosslinked PBD (a) for different angular frequencies and (b) at different temperatures.

shear thinning properties, the developed syntactic foam could be implemented in many applications, including artificial muscles, shock absorbers, and sealants, which can be potentially manufactured by 3D printing.

CRediT authorship contribution statement

SS: Conducting experiments and Writing – original draft; **XF:** Conducting experiments; **GL:** Conceptualization, Methodology, Funding acquisition, and Writing – original draft.

Declaration of Competing Interest

The authors declare that they have no known competing financial interests or personal relationships that could have appeared to influence the work reported in this paper.

Acknowledgments

This work is supported by the National Science Foundation under Grant no. OIA-1946231 and the Louisiana Board of Regents for the

Louisiana Materials Design Alliance (LAMDA), and National Science Foundation under Grant no. 1736136.

Appendix A. Supporting information

Supplementary data associated with this article can be found in the online version at doi:10.1016/j.mtcomm.2022.103303.

References

- M. Harper, G. Li, A review of stimuli-responsive shape memory polymer composites, Polymer 54 (2013) 2199–2221, https://doi.org/10.1016/j. polymer.2013.02.023.
- [2] D.L. Thomsen, P. Keller, J. Naciri, R. Pink, H. Jeon, D. Shenoy, B.R. Ratna, Liquid crystal elastomers with mechanical properties of a muscle, Macromolecules 34 (2001) 5868–5875, https://doi.org/10.1021/ma001639q.
- [3] M. Bothe, T. Pretsch, Two-way shape changes of a shape-memory poly (ester urethane), Macromol. Chem. Phys. 213 (2012) 2378–2385, https://doi.org/ 10.1002/macp.201200096.
- [4] L. Lu, J. Cao, G. Li, Giant reversible elongation upon cooling and contraction upon heating for a crosslinked cis poly (1, 4-butadiene) system at temperatures below zero celsius, Sci. Rep. 8 (2018) 14233, https://doi.org/10.1038/s41598-018-32436-9.

- [5] G. Li, G. Ji, H. Meng, Shape memory polymer-based sealant for a compression sealed joint, J. Mater. Civ. Eng. 27 (2015), 04014196, https://doi.org/10.1061/ (ASCE)MT.1943-5533.0001150.
- [6] G. Li, T. Xu, Thermomechanical characterization of shape memory polymer–based self-healing syntactic foam sealant for expansion joints, J. Transp. Eng. 137 (2011) 805–814, https://doi.org/10.1061/(ASCE)TE.1943-5436.0000279.
- [7] C. Yan, G. Li, A mechanism-based four-chain constitutive model for enthalpy-driven thermoset shape memory polymers with finite deformation, J. Appl. Mech. 87 (2020), 061007, https://doi.org/10.1115/1.4046583.
- [8] Q. Yang, J. Fan, G. Li, Artificial muscles made of chiral two-way shape memory polymer fibers, Appl. Phys. Lett. 109 (2016), 183701, https://doi.org/10.1063/ 1.4966231
- [9] G. Li, Self-healing Composites: Shape Memory Polymer Based Structures, John Wiley & Sons. 2014.
- [10] S.T. Lee, C.B. Park, N.S. Ramesh, Polymeric Foams: Science and Technology, CRC press, 2006.
- [11] L. Wang, Y. Hikima, M. Ohshima, A. Yusa, S. Yamamoto, H. Goto, Unusual fabrication of lightweight injection-molded polypropylene foams by using air as the novel foaming agent, Ind. Eng. Chem. Res. 57 (2018) 3800–3804, https://doi. org/10.1021/acs.iecr.7b05331.
- [12] J.W. Lee, C.B. Park, Use of nitrogen as a blowing agent for the production of finecelled high-density polyethylene foams, Macromol. Mater. Eng. 291 (2006) 1233–1244, https://doi.org/10.1002/mame.200600203.
- [13] L.J. Jacobs, M.F. Kemmere, J.T. Keurentjes, Sustainable polymer foaming using high pressure carbon dioxide: a review on fundamentals, processes and applications, Green Chem. 10 (2008) 731–738, https://doi.org/10.1039/ BROISER
- [14] M. Sauceau, J. Fages, A. Common, C. Nikitine, E. Rodier, New challenges in polymer foaming: a review of extrusion processes assisted by supercritical carbon dioxide, Prog. Polym. Sci. 36 (2011) 749–766, https://doi.org/10.1016/j. progpolymsci.2010.12.004.
- [15] X. Han, K.W. Koelling, D.L. Tomasko, L.J. Lee, Continuous microcellular polystyrene foam extrusion with supercritical CO₂, Polym. Eng. Sci. 42 (2002) 2094–2106. https://doi.org/10.1002/pen.11100.
- [16] H. Tobushi, K. Okumura, M. Endo, S. Hayashi, Thermomechanical properties of polyurethane-shape memory polymer foam, J. Intell. Mater. Syst. Struct. 12 (2001) 283–287. https://doi.org/10.1106/FNSX-AP9V-OP1R-NMWV.
- [17] W. Huang, C. Lee, H. Teo, Thermomechanical behavior of a polyurethane shape memory polymer foam, J. Intell. Mater. Syst. Struct. 17 (2006) 753–760, https://doi.org/10.1177/1045389X06055768.
- [18] M.A. Di Prima, M. Lesniewski, K. Gall, D. McDowell, T. Sanderson, D. Campbell, Thermo-mechanical behavior of epoxy shape memory polymer foams, Smart Mater. Struct. 16 (2007) 2330–2340, https://doi.org/10.1088/0964-1726/16/6/
- [19] F. Zhang, T. Zhou, Y. Liu, J. Leng, Mapping sites of aspirin-induced acetylations in live cells by quantitative acid-cleavable activity-based protein profiling (QA-ABPP). Sci. Rep. 5 (2015) 1–12. https://doi.org/10.1038/srep07896.
- [20] F. Xie, L. Huang, Y. Liu, J. Leng, Synthesis and characterization of high temperature cyanate-based shape memory polymers with functional polybutadiene/acrylonitrile, Polymer 55 (2014) 5873–5879, https://doi.org/ 10.1016/j.polymer.2014.07.035.

- [21] G. Li, D. Nettles, Thermomechanical characterization of a shape memory polymer based self-repairing syntactic foam, Polymer 51 (2010) 755–762, https://doi.org/ 10.1016/j.polymer.2009.12.002.
- [22] P. Zhang, B. Ogunmekan, S. Ibekwe, D. Jerro, S.S. Pang, G. Li, Healing of shape memory polyurethane fiber-reinforced syntactic foam subjected to tensile stress, J. Intell. Mater. Syst. Struct. 27 (2016) 1792–1801, https://doi.org/10.1177/ 1045389X15610912.
- [23] T. Xu, G. Li, A shape memory polymer based syntactic foam with negative Poisson's ratio, Mater. Sci. Eng. A 528 (2011) 6804–6811, https://doi.org/ 10.1016/j.msea.2011.05.034.
- [24] L. Lu, J. Cao, G. Li, A polycaprolactone based syntactic foam with bidirectional reversible actuation, J. Appl. Polym. Sci. 134 (2017) 45225, https://doi.org/ 10.1002/app.45225.
- [25] M. John, G. Li, Self-healing of sandwich structures with a grid stiffened shape memory polymer syntactic foam core, Smart Mater. Struct. 19 (2010), 075013, https://doi.org/10.1088/0964-1726/19/7/075013.
- [26] G. Li, V.D. Muthyala, Impact characterization of sandwich structures with an integrated orthogrid stiffened syntactic foam core, Compos. Sci. Technol. 68 (2008) 2078–2084, https://doi.org/10.1016/j.compscitech.2008.03.014.
- [27] P. Mylavarapu, G. Li, N. Gupta, R. Maharsia, E. Woldesenbet, Ultrasonic signal attenuation in syntactic foams filled with rubber particles, ASME Int. Mech. Eng. Congr. Expo. 47160 (2004) 25–29, https://doi.org/10.1115/IMECE2004-59375.
- [28] J. Fan, G. Li, High enthalpy storage thermoset network with giant stress and energy output in rubbery state, Nat. Commun. 9 (2018) 642, https://doi.org/10.1038/ 041477 018 0204 2
- [29] C. Yan, Q. Yang, G. Li, A phenomenological constitutive model for semicrystalline two-way shape memory polymers, Int. J. Mech. Sci. 177 (2020), 105552, https://doi.org/10.1016/j.ijmecsci.2020.105552.
- [30] L. Lu, G. Li, One-way multishape-memory effect and tunable two-way shape memory effect of ionomer poly(ethylene-co-methacrylic acid), ACS Appl. Mater. Interfaces 8 (2016) 14812–14823, https://doi.org/10.1021/acsami.6b04105.
- [31] J. Fan, G. Li, High performance and tunable artificial muscle based on two-way shape memory polymer, RSC Adv. 7 (2017) 1127–1136, https://doi.org/10.1039/ C6RA25024F.
- [32] E. Riande, R. Diaz-Calleja, M. Prolongo, R. Masegosa, C. Salom, Polymer Viscoelasticity: Stress and Strain in Practice, CRC Press, 1999.
- [33] W. Xu, G. Li, Constitutive modeling of shape memory polymer based self-healing syntactic foam, Int. J. Solids Struct. 47 (2020) 1306–1316, https://doi.org/ 10.1016/j.jisolstr.2010.01.015.
- [34] G. Li, Y. Zhao, S.S. Pang, A three-layer built-in analytical modeling of concrete, Cem. Concr. Res. 28 (1998) 1057–1070, https://doi.org/10.1016/S0008-8846(98) 00062-3
- [35] N. Gupta, R. Nagorny, Tensile properties of glass microballoon-epoxy resin syntactic foams, J. Appl. Polym. Sci. 102 (2006) 1254–1261, https://doi.org/ 10.1002/app.23548.
- [36] J.P. Lin, C.Y. Chang, C.H. Wu, S.M. Shih, Thermal degradation kinetics of polybutadiene rubber, Polym. Degrad. Stab. 53 (1996) 295–300, https://doi.org/ 10.1016/0141-3910(96)00098-5.
- [37] W. Schnabel, G.F. Levchik, C.A. Wilkie, D.D. Jiang, S.V. Levchik, Thermal degradation of polystyrene, poly (1, 4-butadiene) and copolymers of styrene and 1, 4-butadiene irradiated under air or argon with ⁶⁰Co-γ-rays, Polym. Degrad. Stab. 63 (1999) 365–375, https://doi.org/10.1016/S0141-3910(98)00114-1.